ACADEMIC PRESS

Available online at www.sciencedirect.com

SCIENCE DIRECT®

Journal of Sound and Vibration 265 (2003) 1025–1045

JOURNAL OF SOUND AND VIBRATION

www.elsevier.com/locate/jsvi

Suppression of flow–acoustic coupling in sidebranch ducts by interface modification

B.D. Knotts, A. Selamet*

Department of Mechanical Engineering, The Ohio State University, 206 West 18th Ave., Columbus, OH 43210-1107, USA

Received 24 July 2000; accepted 20 August 2002

Abstract

The flow–acoustic coupling of shear layer instabilities with the acoustic resonances at the interface of a closed sidebranch and main duct can produce high-amplitude pure-tone noise, known as "whistle". This study investigates experimentally the effect of various interface geometry modifications on whistles. The objective of the modifications is to suppress the noise by redirecting the shear layer at the main duct–sidebranch interface. Interchangeable suppressor blocks of varying shapes and sizes mounted upstream and downstream of the sidebranch opening are used to change the geometry. The block shapes include those with square edges, ramps, bevelled edges, and curved (radiused) edges. The experiments are conducted in a flow facility at conditions that include certain ranges of Strouhal numbers known to coincide with significant noise generation. The effectiveness of various suppressors in reducing the noise is assessed by analyzing the measured sound pressure levels.

1. Introduction

Quarter-wave resonators are often utilized in various applications to suppress noise within certain frequency ranges. The mean flow across the opening of the duct, however, forms an unsteady shear layer that may interact with acoustic waves in the sidebranch. Under certain flow and geometry conditions, these disturbances in the shear layer are then coupled with the acoustic waves, thereby generating a feedback mechanism, which produces high-amplitude pure-tone whistles. This flow–acoustic coupling phenomenon can produce pressure oscillations in the sidebranch with amplitudes above 150 dB and distinct vortices near the sidebranch opening. The former produces a significant oscillating force on, for example, valves, resulting in diaphragm fluctuations combined with a chattering noise. The latter leads to loud, disturbing pure-tone

*Corresponding author. Tel.: +614-292-2289; fax: +614-292-3163.
E-mail address: selamet.1@osu.edu (A. Selamet).

0022-460X/03/$ - see front matter
doi:10.1016/S0022-460X(02)01254-3

whistles at discrete frequencies that propagate through the main duct. To suppress the resulting large-amplitude pressure oscillations, the feedback mechanism present at the main duct–sidebranch interface needs to be interrupted. One method of interruption is to stabilize the shear layer and prevent it from forming large-scale vortices, which can be accomplished by redirecting it with modifications to the geometry of the main duct–sidebranch interface. The objective of these modifications is to reduce the amplitude of pressure oscillations without acting as a source of significant noise.

The study of cavity flows and flow noise has produced a significant amount of literature. Rockwell and Naudascher [1] and Komerath et al. [2] provide extensive general reviews. While there are numerous works available on the mechanism of flow–acoustic coupling, only a few have concentrated on the means of suppressing the generated noise. Also, the majority of the works on suppression have focused on shallow cavities where the cavity length to width ratio L/d, as shown in Fig. 1, is less than unity, such as aircraft bomb bays. Franke and Carr [3] examined shallow cavities with various configurations of ramps and bevels at the cavity opening. All of their tests were performed at Mach numbers $Ma > 1.0$. They found that a combination of bevels upstream and downstream of the sidebranch opening effectively suppressed pressure oscillations for certain cavity sizes, but were ineffective for other cavities. Using only a downstream bevel with an upstream sharp edge was rarely effective, and the location of flow separation on the bevel was important in determining its effectiveness. They also examined different sizes of upstream ramps

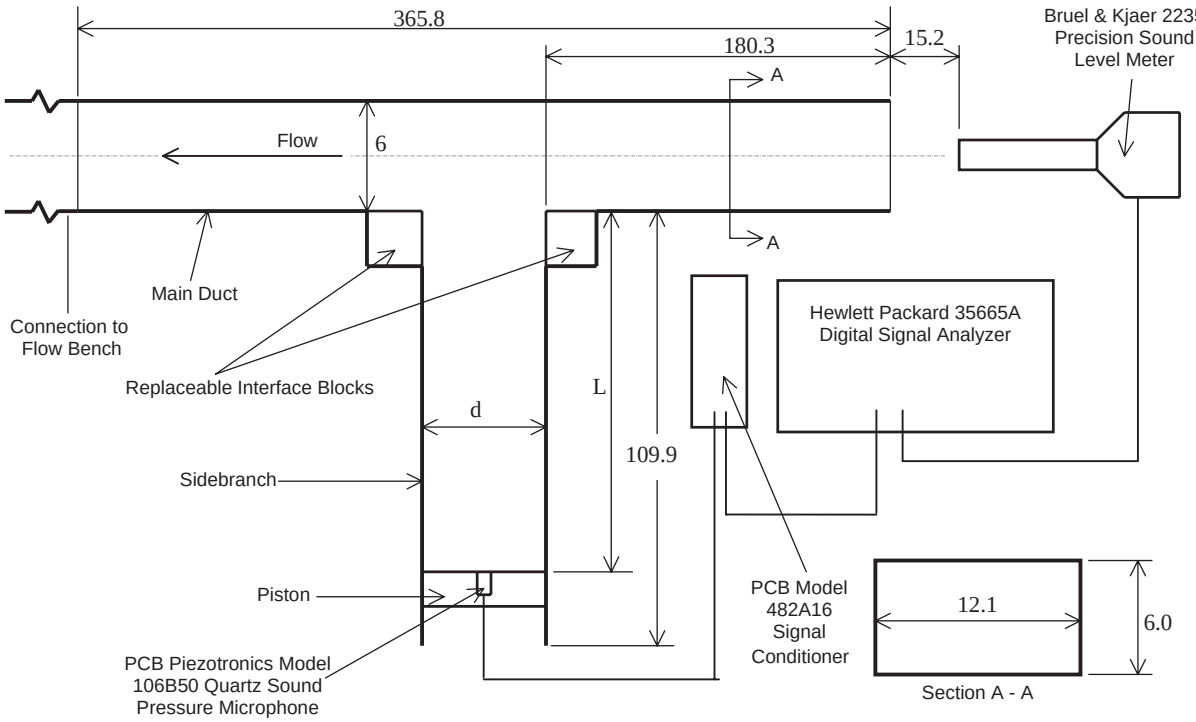

Fig. 1. Schematic of experimental set-up, $d = 2$ cm (all dimensions in cm; schematic not to scale).

with downstream sharp edges and found that the ramps considerably lowered the amplitude of pressure oscillations for the cavities tested. Heller and Bliss [4] also investigated shallow cavities in a wind tunnel for $Ma = 0.8$–2.0. A downstream 45° bevel was examined by itself and in combination first with upstream spoilers, then with a detached cowl. The combination of the bevel and spoilers provided the most suppression, although the bevel alone worked well for the more shallow cavities examined. The detached cowl placed just above the bevel also suppressed the amplitude of oscillations well, particularly for the relatively deeper cavities tested. Heller and Bliss noted, however, that the position of the cowl was critical to providing optimum suppression. Shaw [5] conducted a similar study to Heller and Bliss with similar results, only instead of a wind tunnel the testing was performed using a shallow cavity in an aircraft weapons pod that was flight tested at $Ma = 0.6$–1.3. Sarno and Franke [6] fixed a 0.1 in tall fence directly upstream of a shallow cavity opening to act as a flow obstacle and tested the set-up at $Ma = 0.6$–1.6. The fence only proved effective at suppressing the first vortex mode at higher Mach numbers such as 1.28 and 1.53. The fence was relatively ineffective at suppressing the first mode at lower Ma and the second mode for all Ma. Sarno and Franke also used a pulsating height fence to try to force the shear layer at a different frequency than the resonant frequency of the shallow cavity. The pulsating fence reduced some amplitudes but caused a high-amplitude peak at the fence pulsation frequency.

A limited number of works have focused on suppression methods for deep cavities such as sidebranches. Baldwin and Simmons [7] studied sidebranches in the form of safety relief valves (SRVs) as used in power plant pipes. They found that all of the valves studied with vibration problems due to flow–acoustic coupling were operating in a Strouhal number range of 0.3–0.6. To reduce SRV vibration problems, they suggested to avoid the St range where the problem occurred, and to stabilize the shear layer by changing the valve design by either rounding the edges of the sidebranch opening or bevelling the edges at a 45° angle.

Jungowski et al. [8] studied cylindrical sidebranches of varying diameters and lengths. The normalized branch diameters d/D_{main} (where D_{main} is the main duct diameter) ranged from 0.136 to 1.0 with branch lengths varying from 0.025 to 1.7 m. The experiments were conducted using flow velocities covering $Ma = 0.025$–0.2. The edges of the sidebranch entrance were also radiused with normalized radii r/d from 0 to 0.6. They found that, with sharp sidebranch edges (no radius), the maximum tone amplitudes occurred in two modes, the first at $St = 0.2$–0.55 and the second at approximately double the St of the first mode. The amplitudes at the closed end of the sidebranch also increased with increasing Ma. The second mode generally had a lower amplitude than the first. Adding a radius to the edges of the main duct–sidebranch interface lowered the frequency and the St of the peak amplitudes with increasing radius. Increasing d/D_{main} over 0.2 and r/d above 0.1 reduced the maximum tone amplitudes, whereas for $r/d = 0.1$ the amplitudes slightly increased.

Bruggeman et al. [9] examined the effects of radiusing the edges of the main duct–sidebranch interface and placing various spoilers in single and double sidebranch set-ups. The radiused edges reduced the amplitude of pressure oscillations in the single sidebranch set-up, with the amplitude reduction increasing with radius. In the double sidebranch set-up, however, radiusing the edges did not always reduce the pressure amplitudes. The spoilers consisted of various arrangements of teeth placed in the main duct upstream of the sidebranch or over the sidebranch opening. Placing spoilers at the upstream edge of the sidebranch below a critical ambient pressure reduced the

amplitude of pressure oscillations. Hysteresis in the effectiveness of the spoilers with changing pressure was observed above the critical pressure, indicating a non-linear behavior.

McGrath and Olinger [10] considered a control screen placed inside a square, deep sidebranch with open area varying from 30% to 70%. Covering a range of $L/d = 3.94$–7.19, and flows at relatively low Ma, their set-up also incorporated microphones mounted along the length L to determine the root mean square pressure distribution of standing acoustic waves in the sidebranch. With a proper positioning of the porous screen (at the velocity fluctuation maxima), they achieved peak suppressions at the closed end of the cavity as high as 26 dB for the coupled single vortex and the first quarter-wave acoustic wave modes.

Some of the foregoing researchers [3–6] have concentrated on shallow cavities and relatively high Mach numbers, while others [7–10] have investigated predominantly the effect of interface edge rounding, spoilers, and screens at lower Mach numbers. A simultaneous examination of several suppressors using the same experimental set-up remains desirable to achieve a comparative assessment of their effectiveness. The objective of the present experimental study is then to provide a systematic investigation of a number of main duct–sidebranch interface modifications on flow–acoustic noise at low Mach numbers ($Ma < 0.3$) representative of reciprocating machinery, including internal combustion engines and compressors. A two-dimensional experimental set-up has been built from clear acrylic consisting of a rectangular main duct with a connected closed sidebranch. The main duct–sidebranch interface is modified by using interchangeable blocks of varying shapes and sizes, including blocks with square edges as a baseline, and three different suppressors considered here: ramps, bevelled edges, and radiused edges [11]. The width and length of the sidebranch can be varied using a movable piston, which closes the end of the sidebranch. The experiments are conducted on a flow stand at a range of flow rates, including those that correspond to certain ranges of Strouhal numbers known to coincide with significant noise generation due to flow–acoustic coupling. The sound pressure level is measured at the inlet of the main duct and on the surface of the piston. The results are analyzed to determine the effectiveness of three suppressors in reducing the flow–acoustic noise.

Following this introduction Section 2 describes the experimental set-up, procedures, and method of data analysis. Section 3 provides the results for sharp edge (or square) interface blocks to establish the baseline data for comparison to the suppressor blocks that follow. The baseline results are subsequently compared with those of three suppressors examined: ramps, bevels, and radius (curved) interfaces, in Sections 4–6, respectively. The study is concluded in Section 7 with some final remarks.

2. Experimental set-up

The experimental set-up consists of a rectangular main duct with a connected closed sidebranch as shown in Fig. 1. The main duct is 365.8 cm long with the upstream edge of the sidebranch 180.3 cm from the inlet. The inner dimensions of the main duct are 12.1 cm high by 6.0 cm wide, while the inner height of the sidebranch is also 12.1 cm with an adjustable width. A rectangular set-up is chosen to assist a computational work [12] and for ease of changing the main duct–sidebranch interface geometry. A rectangular piston machined from PVC closes the end of the sidebranch. The sidebranch length L can be modified by moving the piston, while the width d can

be changed by using a different size piston and moving the downstream side of the sidebranch. The set-up is constructed using 1.27 cm thick clear acrylic sheet held together with cap screws. Any portion of the assembly that must be removable to allow for the movement of piston is held in place with threaded studs and wing nuts. The seams between the acrylic sheets are sealed airtight with circular rubber O-rings fitted into grooves. The main duct is connected to a flow bench with an electric-motor driven turbine that induces steady flow rates up to 1100 cubic feet per minute (cfm) in the direction shown in Fig. 1. Table 1 lists the flow rates used, along with the corresponding main duct velocity U, Ma, and Reynolds number $Re = UD_H/v$, for a typical laboratory air temperature of 70°F, where D_H is the hydraulic diameter of the main duct and v is the kinematic viscosity.

Interchangeable blocks made from PVC are mounted upstream and downstream of the main duct–sidebranch interface. These blocks are used to modify the geometry of the interface through changes in their shape from the square cross-section in Fig. 1. Four different types of blocks are used in various combinations for the experiments: square, ramp, bevel, and radius (curved). The square blocks (6 cm × 6 cm × 12.1 cm) produce a sharp-edged right angle interface, as illustrated in Fig. 1, which provides baseline results for comparison with the other blocks. Fig. 2 shows examples of how each of the different types of blocks are mounted at the interface in the experimental set-up. The ramp heights used are $h = 0.25$, 0.5, 1.0, and 1.5 cm, with the ramp length a chosen so that $a/h = 3$ for all blocks. The bevel blocks use bevel drops of $h = 0.25$, 0.5, 1.0, and 1.5 cm, and the bevel length a chosen so that $a/h = 3$ for all of the blocks. The rounded edges of the radius blocks are formed using one of four different radii: $r = 0.5$, 1.0, 1.5, and 2.0 cm. All of the experiments use a sidebranch width of 2 cm since this dimension is representative of sidebranches in actual engine hardware such as the throttle body and intake manifolds.

The data recorded for each experiment consists of the unweighted sound pressure level [$SPL = 20 \log_{10} p_{r.m.s.}/(2 \times 10^{-5})$, $p_{r.m.s.}$ being root mean square pressure in Pa] at the inlet of the main duct and on the surface of the piston. The inlet measurement is made using a Bruel & Kjaer (B&K) 2235 Precision Sound Level Meter (SLM) with a 0.5 in diameter B&K 4176 Prepolarized Condenser Microphone. The SLM is positioned 15.2 cm (6 in) outside the main duct inlet aligned with the main duct centerline axis as shown in Fig. 1. The SLM is calibrated using a B&K 4230

Table 1
Discrete flow rates, mean velocities, Ma, and Re used in the experiment

Flow rate (cfm)	Mean velocity (m/s)	Ma	Re
300	19.6	0.057	9.928×10^4
400	26.2	0.076	1.324×10^5
500	32.8	0.095	1.655×10^5
600	39.3	0.114	1.986×10^5
700	45.9	0.133	2.316×10^5
800	52.4	0.153	2.647×10^5
900	59.0	0.172	2.978×10^5
1000	65.5	0.191	3.309×10^5
1100	72.1	0.210	3.640×10^5

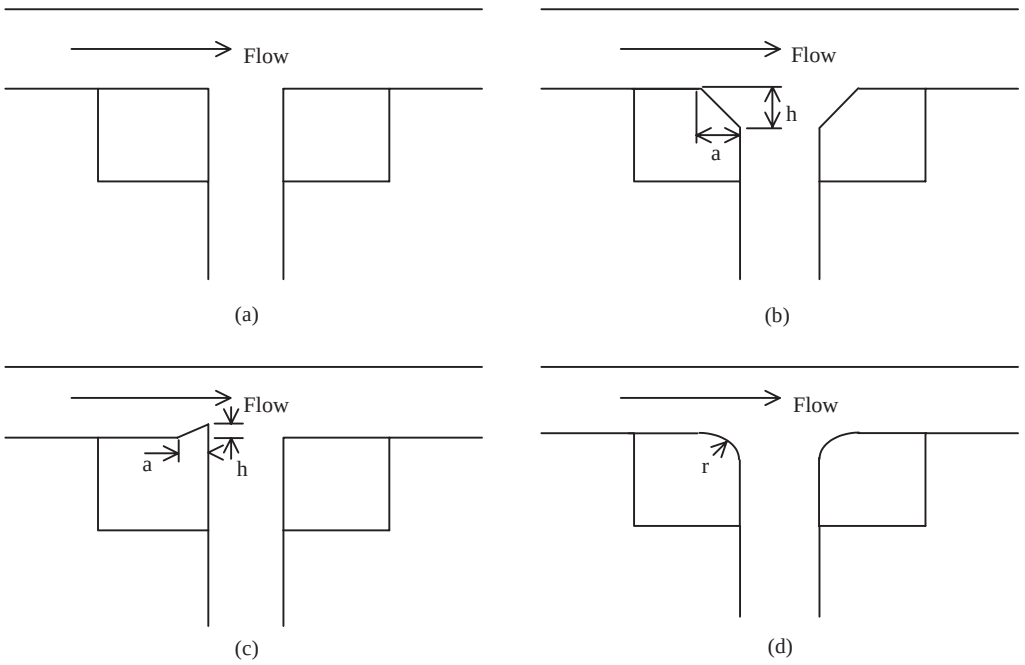

Fig. 2. Schematics of block configurations at main duct–sidebranch interface in experimental set-up ($a/h = 3$): (a) square blocks upstream and downstream; (b) bevel blocks upstream and downstream; (c) ramp block upstream, square block downstream; (d) radius blocks upstream and downstream.

Pistonphone that produces a calibration signal of 93.8 dB at 1 kHz. The measurements at the piston surface use a PCB Piezotronics Model 106B50 Quartz Sound Pressure Microphone flush-mounted at the center of the piston along the axis of the sidebranch. A PCB Model 482A16 Signal Conditioner is used to amplify the piston transducer signal. The inlet signal from the SLM and the amplified signal from the piston transducer are sent on separate channels to a Hewlett-Packard 35665A Digital Signal Analyzer (DSA). The DSA acquires the data at an 8 Hz resolution, giving a total of 800 points collected over a frequency range of 0–6.4 kHz, and ensemble averages the acquired data over 15 cycles.

Before each experiment the interface blocks are installed and the piston is set so that $L = 1.0$ m. The flow bench is then turned on, and once the flow stabilizes at the first set point (300 cfm) the data is recorded. This procedure is then repeated in 100 cfm intervals up to a flow rate of 1100 cfm. The piston is subsequently moved in 0.1 m intervals to $L = 0.1$ m and then to $L = 0.05$ m and the process is repeated for each flow rate. Such a variation in sidebranch length yields a range of $L/d = 2.5$–50 for deep cavities investigated in the present work. An additional set of experiments is conducted using the square blocks with the piston set at $L = 0$ m, at which the piston face is flush with the floor of the main duct to provide a background noise measurement. The ambient room temperature is measured at the beginning and end of each set of experiments and then averaged to determine the mean temperature for the calculation of the speed of sound. The typical temperature variance during the experiment is less than 3°F, resulting in a variance of less than 1% in the speed of sound.

3. Sharp-edged interface results

These experiments have been conducted using the square blocks that create a sharp-edged right angle main duct–sidebranch interface as shown in Fig. 1. The objective is to produce a baseline to be compared with different types of suppressors. The experiments follow the procedure detailed in the preceding section. The $p_{r.m.s.}$ (Pa) measurements are first converted to SPL in dB. The results for a particular sidebranch length and flow rate are then depicted as SPL against frequency spectrum by a solid line, as illustrated by an example in Fig. 3. The data for the zero-length sidebranch background noise experiment at the same flow rate is superimposed on the same figure by a dashed line. The comparison then identifies the solid-line peaks in Fig. 3 that are due to the sidebranch length and main duct–sidebranch interface configuration, different than background noise. For example, the three peaks at frequencies of 1200, 2400, and 3600 Hz in Fig. 3 are clearly due to the sidebranch length of $L = 0.2$ m since the solid line representing these peaks is much higher in SPL than the $L = 0$ m case. The spectra for each flow rate and sidebranch length are examined, and the frequency and maximum amplitude of any peak more than 5 dB higher than the background noise are noted. For each of these selected peaks, the flow velocity, Strouhal number, Mach number, and normalized frequency are then calculated. The Strouhal number St and Mach number Ma are determined by

$$St = \frac{fd}{U} \tag{1}$$

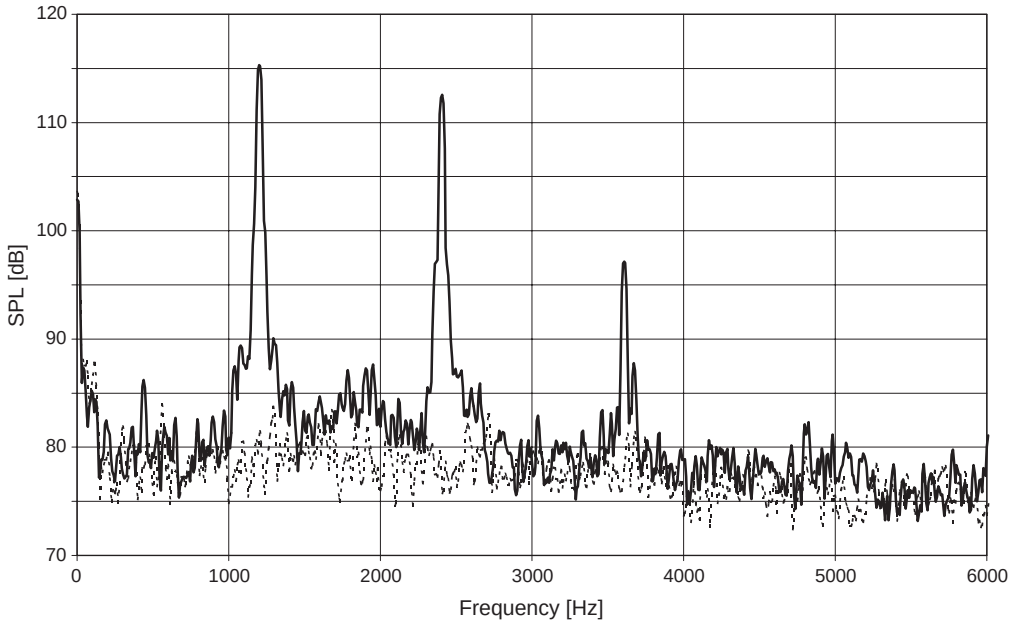

Fig. 3. Typical frequency spectra for inlet SPL from SLM: comparison of (——) and $L = 0$ m (- - - - - -) measurements, 1100 cfm.

and

$$Ma = \frac{U}{c}, \tag{2}$$

where f (Hz) is the frequency of the measured peak, d (m) is the sidebranch width, U (m/s) is the average velocity in the main duct obtained from the volumetric flow rate measurements, and $c = \sqrt{\gamma RT}$ (m/s) is the speed of sound, $\gamma = 1.4$ being the specific heat ratio and $R = 287\,\mathrm{J/kg\,K}$ the specific gas constant for air, and T (K) the measured air temperature. The measured peak frequencies are normalized by the first quarter-wave frequency as

$$f_n = \frac{f}{c/4L_c}, \tag{3}$$

where f_n will hereafter be referred to as the normalized frequency and

$$L_c = L + 0.85\frac{d}{2} \tag{4}$$

is the sidebranch length with end correction corresponding to Rayleigh's upper limit [13] and L is the measured sidebranch length. All calculations involving the sidebranch length utilize the end correction given by Eq. (4). These results are then shown by individual points on *SPL* against *St*, *St* against *Ma*, *SPL* against *Ma*, frequency against *Ma*, and *SPL* against f_n graphs, with each point representing an *SPL* range or sidebranch length. These "dot graphs" provide the basis for the analysis and comparison of the three different suppressors to be discussed in the following sections.

The peak *SPL* measured by the SLM outside the main duct inlet (recall Fig. 1) against *St* data in Fig. 4 provides an overview of the *St* range of the noise peaks caused by the sidebranch. The strongest band of peaks is centered at $St = 0.4$, while a secondary band is centered at about $St = 0.7$. The lower *St* band has a higher maximum amplitude (about 120 dB) than the higher *St* band with a maximum amplitude of about 115 dB. This trend suggests the first vortex mode peaks, which make up the lower *St* band are generally the strongest, with the subsequent second mode peaks in the higher *St* band weakening in amplitude. The dashed lines represent approximate envelopes for the square block peaks, and will be repeated in corresponding graphs for comparison. Fig. 5, which depicts the peak frequency against *Ma*, reveals two distinct bands of high-amplitude (greater than 100 dB) points. Each of these bands increases in frequency with increasing *Ma*. These trends are explained by the definition of *St* in Eq. (1), which implies that to maintain a constant *St* the frequencies of the peaks must increase with flow velocity, and with decreasing sidebranch width. The peak *SPL* against f_n is shown in Fig. 6. In view of the fact that quarter-wave frequencies for small-amplitude waves are given by $f_q = (2n+1)c/4L_c$, $n = 0, 1, 2, \ldots, f_n$ is expected to be an odd integer when measured peak frequencies agree with the quarter-wave frequencies. Fig. 6 shows that a substantial number of peaks do have f_n that are odd integers, particularly those with dominant *SPL* (> 100 dB), indicating the presence of strong flow–acoustic coupling. Recently, the details of such a strongly coupled interface physics, including the vortex motion, have been effectively illustrated by a computational fluid dynamics approach [12]. The peaks that do not have odd integer f_n could partially be attributed to other sources, including resonances in the main duct inlet, and non-linearities resulting in multiple frequencies of strong flow–acoustic peaks. For example, in Fig. 3 the 115 dB peak has a frequency of 1200 Hz, which

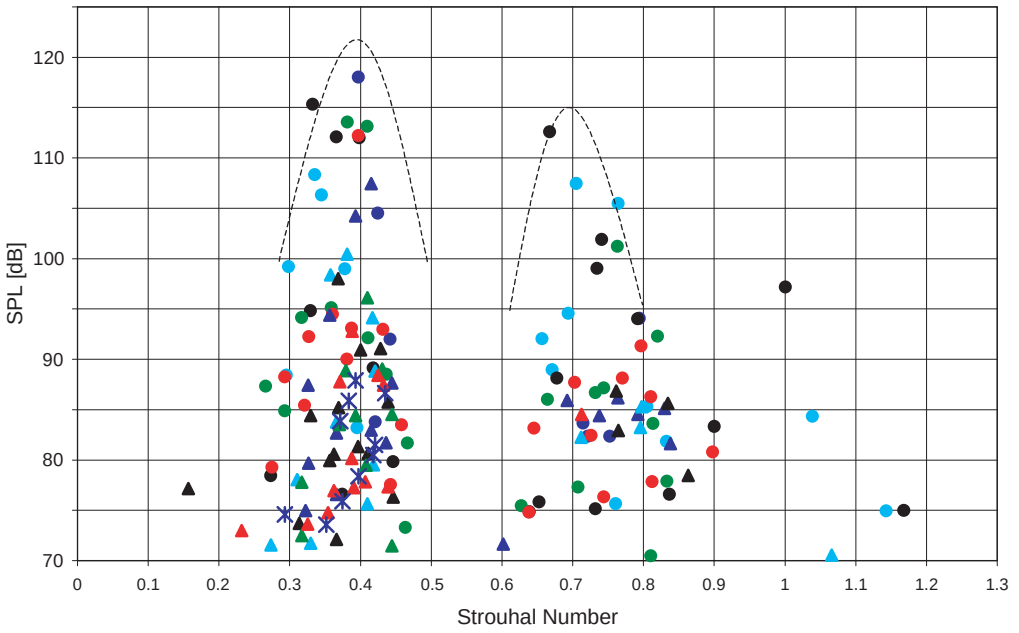

Fig. 4. Inlet *SPL* versus Strouhal number; variable sidebranch lengths, square edges; length *L*: ●, 0.05 m; ●, 0.1 m; ●, 0.2 m; ●, 0.3 m; ●, 0.4 m; ▲, 0.5 m; ▲, 0.6 m; ▲, 0.7 m; ▲, 0.8 m; ▲, 0.9 m; ✳, 1.0 m.

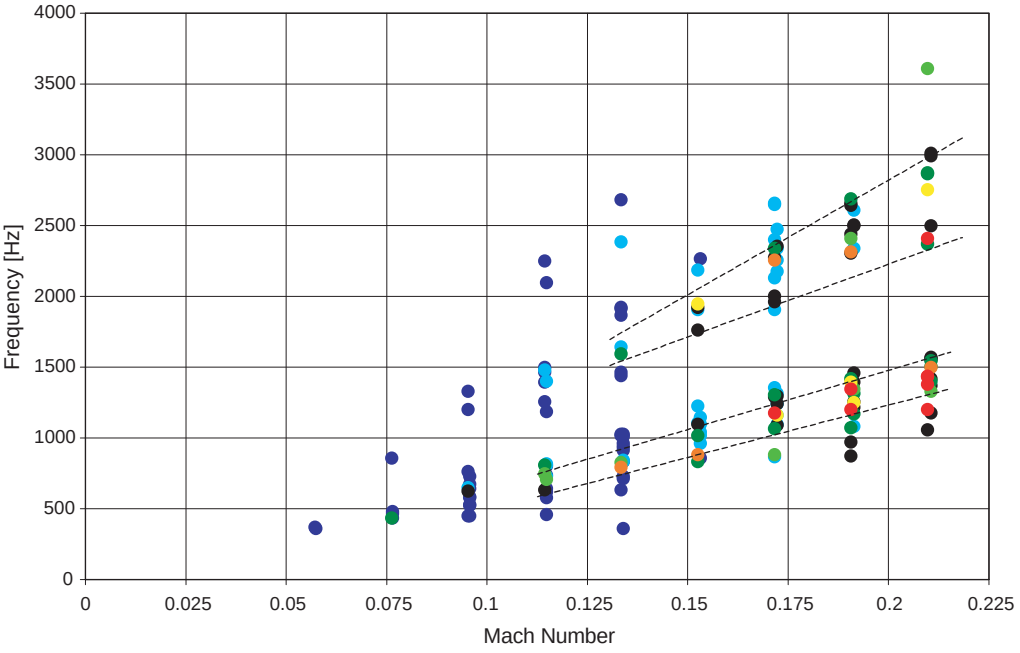

Fig. 5. Inlet frequency versus Mach number; variable sidebranch lengths, square edges; amplitude: ●, 70–80 dB; ●, 80–85 dB; ●, 85–90 dB; ●, 90–95 dB; ●, 95–100 dB; ●, 100–105 dB; ●, 105–110 dB; ●, 110–120 dB.

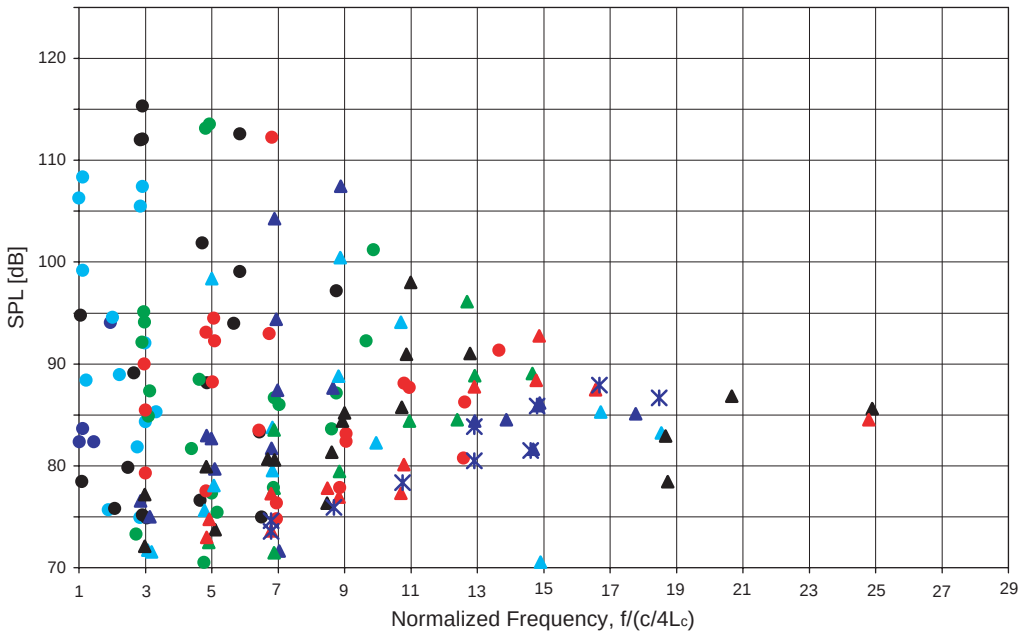

Fig. 6. Inlet *SPL* versus normalized frequency; variable sidebranch lengths, square edges; length, L: ●, 0.05 m; ●, 0.1 m; ●, 0.2 m; ●, 0.3 m; ●, 0.4 m; ▲, 0.5 m; ▲, 0.6 m; ▲, 0.7 m; ▲, 0.8 m; ▲, 0.9 m; ✱, 1.0 m.

corresponds to $3c/4L_c$ for the sidebranch configuration examined. The peaks of 112 dB at 2400 Hz and 97 dB at 3600 Hz correspond to twice and three times the frequency of the peak at 1200 Hz.

As indicated earlier, the results in Figs. 4–6 are based on external *SPL* measurements. The amplitudes measured with the pressure transducer at the piston face follow the same trends as the inlet results, with the only significant difference being the relative magnitudes. As a typical illustration, Fig. 7 compares the piston *SPL* against the inlet *SPL* from Fig. 3 (for $L = 0.2$ m and 1100 cfm) showing that the frequencies of dominant peaks coincide in two measurements, as expected. This relationship between the two locations continues regardless of the type of interface block, including suppressors, therefore the remainder of the paper concentrates on the external measurements.

4. Ramps

The effectiveness of upstream ramps as suppressors has been studied experimentally and the results are presented in this section. The ramps span the full height of the block, and therefore the main duct. The ramp is on the long edge of the block perpendicular to the airflow, and has a triangular shape when viewed from the end of the block as shown in Fig. 2. Each ramp block is mounted in the experimental set-up upstream of the main duct–sidebranch interface so that the ramp directs air away from the sidebranch opening. Following the procedure discussed in Section 2, four experiments are conducted with the ramp heights $h = 0.25$, 0.5, 1.0, and 1.5 cm,

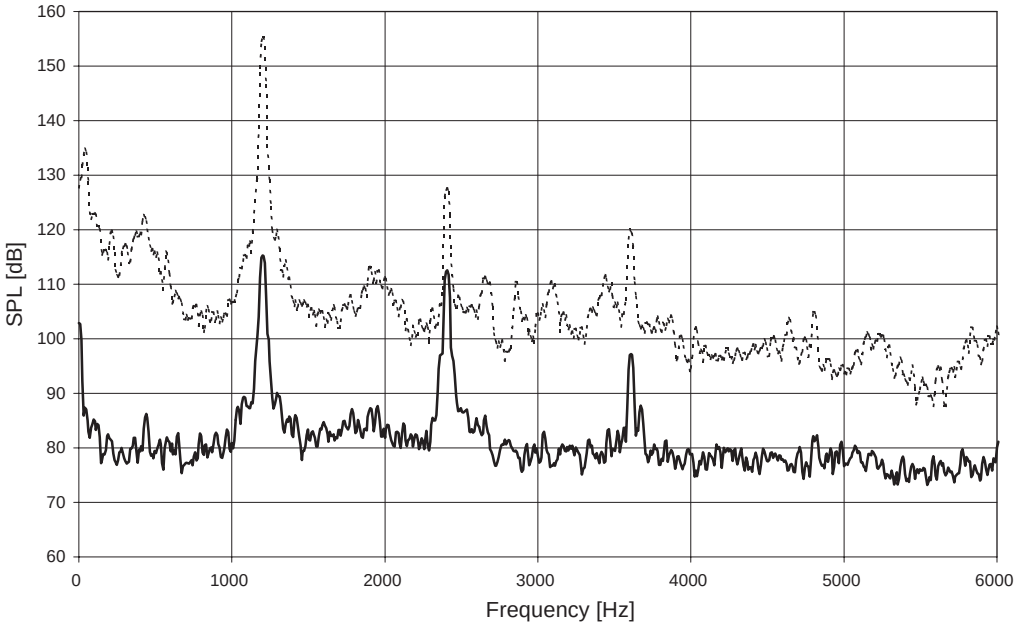

Fig. 7. Comparison of piston (------) and inlet (——) measurements, $L = 0.2$ m, 1100 cfm.

corresponding to $h/d = \frac{1}{8}, \frac{1}{4}, \frac{1}{2}$, and $\frac{3}{4}$, respectively. For each ramp experiment a square block is used in the downstream position.

The results of the ramp experiments are compared with the baseline results that use the sharp-edged square interface blocks in both the upstream and downstream positions. The peaks in Section 3 due to a pair of square blocks are referred to as either "square" or "baseline" peaks. For a selected sidebranch length of $L = 0.2$ m and a flow rate of 1100 cfm, Fig. 8 provides an illustrative comparison of the magnitude spectra from the four ramps examined and the square interface blocks. The square blocks and the $h/d = \frac{1}{8}$ and $\frac{1}{4}$ ramps produce separate high magnitude peaks, such as the one at 1200 Hz due to the square blocks and the peak at 1950 Hz due to the smaller two ramps. For the same L and flow rate, Fig. 9 shows that the frequencies of the dominant peaks in Fig. 8 correlate with the piston surface measurements. Fig. 8 suggests that although the two smaller ramps are effective at suppressing the high SPL baseline peaks, these ramps also create new peaks at different frequencies. These new peaks generally have a higher frequency than the strongest baseline peaks. Fig. 8 also shows that the two larger ramps with $h/d = \frac{1}{2}$ and $\frac{3}{4}$ effectively suppress all of the distinct baseline peaks without creating any new significant peaks.

The increased frequency of the peaks created by the two smaller ramps compared to the strongest baseline peaks can be examined by comparing the normalized frequencies f_n of these peaks. Some of the significant peaks caused by the two smaller ramps have a f_n that is higher by approximately 2 than that of the strongest baseline peak for the same L and flow rate, suggesting that the f_q of these peaks is about 1 mode higher than that of the strongest baseline peaks. For example, $f_n = 2.9$ for the baseline peak at 1200 Hz in Fig. 8, while $f_n = 4.7$ for the ramp peak at about 2000 Hz. This trend is repeated for other sidebranch lengths and flow rates.

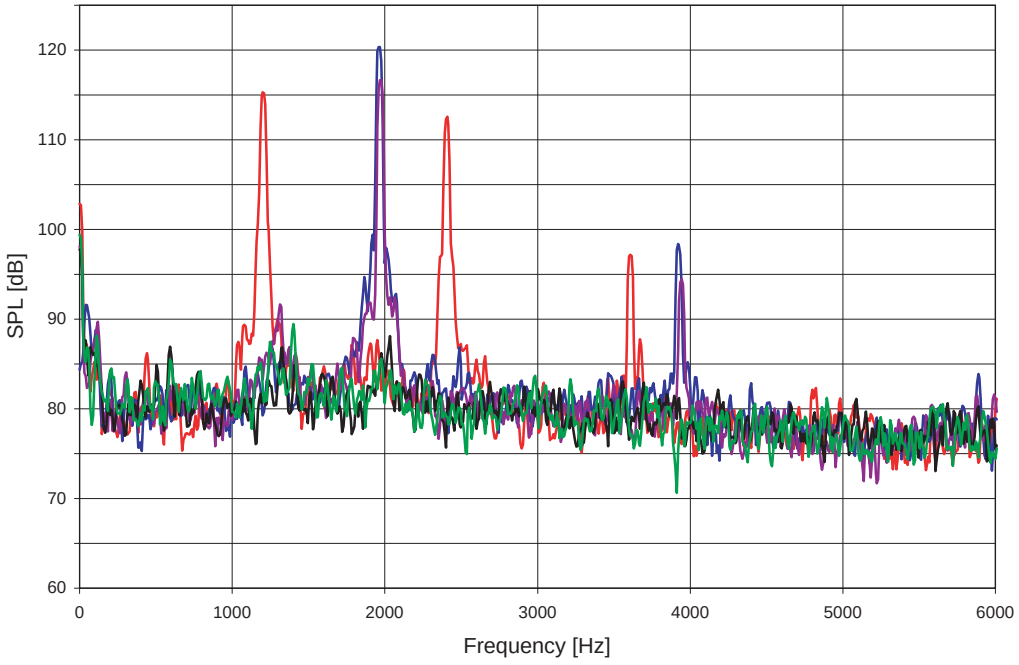

Fig. 8. Inlet *SPL* versus frequency; comparison of square with upstream ramp interfaces, $L = 0.2$ m, 1100 cfm: ——, square; h/d: ——, $\frac{1}{8}$; ——, $\frac{1}{4}$; ——, $\frac{1}{2}$; ——, $\frac{3}{4}$.

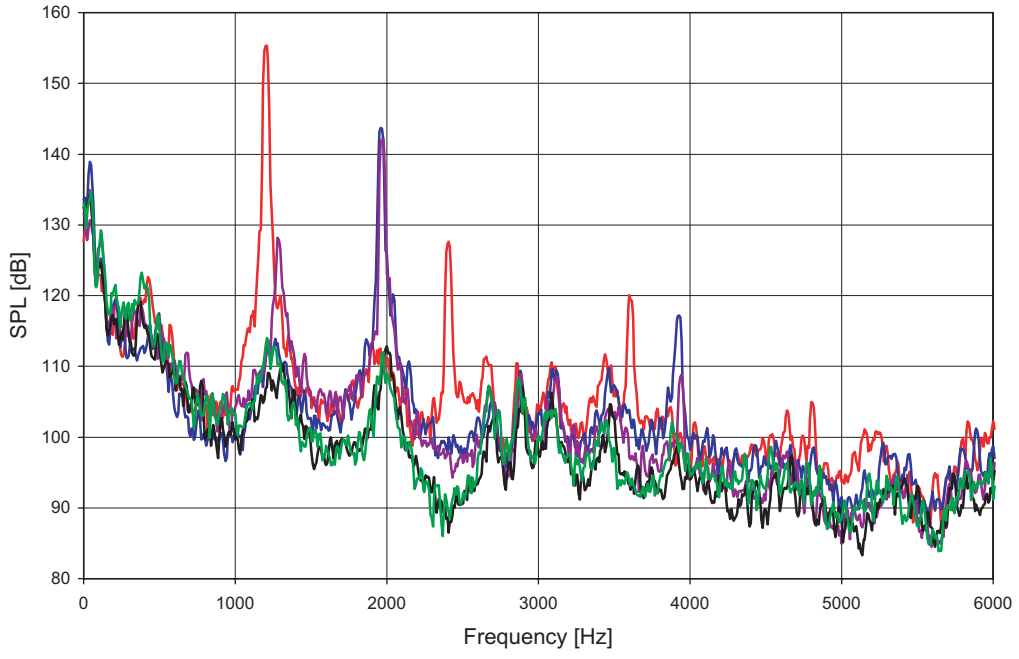

Fig. 9. Piston *SPL* versus frequency; Comparison of square with upstream ramp interfaces, $L = 0.2$ m, 1100 cfm: ——, square; h/d: ——, $\frac{1}{8}$; ——, $\frac{1}{4}$; ——, $\frac{1}{2}$; ——, $\frac{3}{4}$.

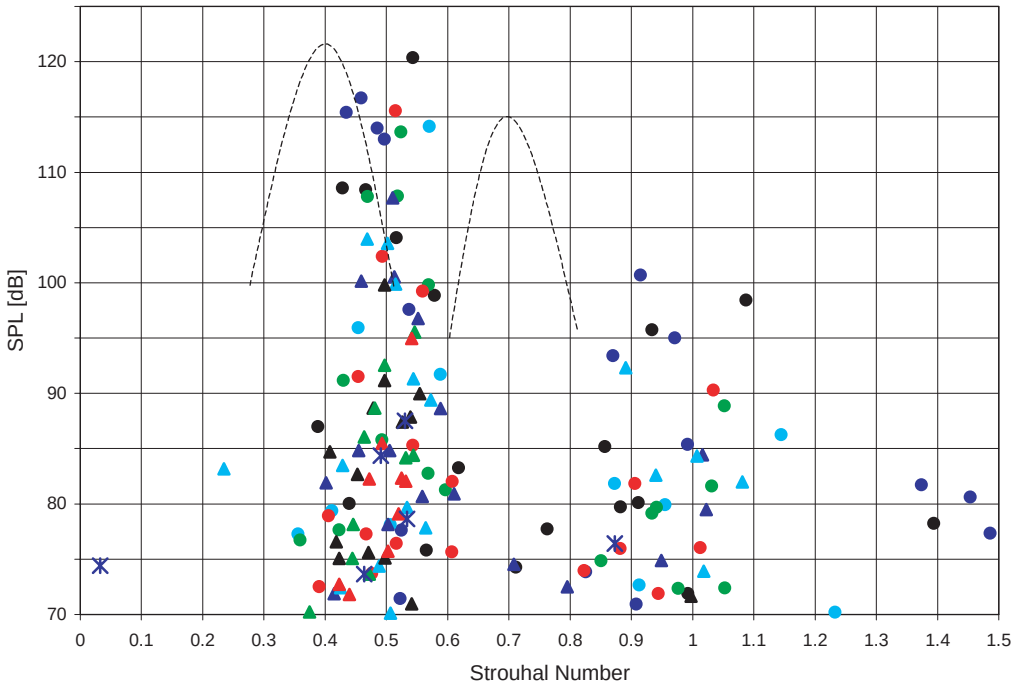

Fig. 10. Inlet *SPL* versus Strouhal number; variable sidebranch lengths, upstream $h/d = \frac{1}{8}$ ramp; length, *L*: ●, 0.05 m; ●, 0.1 m; ●, 0.2 m; ●, 0.3 m; ●, 0.4 m; ▲, 0.5 m; ▲, 0.6 m; ▲, 0.7 m; ▲, 0.8 m; ▲, 0.9 m; ✱, 1.0 m.

Figs. 10 and 11, which represent the *SPL* against Strouhal number for the smallest and largest ramps, may be compared to Fig. 4 for the square interface configuration. As indicated earlier, the dashed lines of Fig. 4 representing the envelopes for square block peaks are superimposed in Figs. 10 and 11 for ease of comparison. The $h/d = \frac{1}{8}$ ramp slightly shifts the strongest band of peaks from $St = 0.4$ in Fig. 4 to $St = 0.5$ in Fig. 10, while eliminating any of the peaks higher than about 100 dB in the weaker band centered around $St = 0.9$. The results for the largest ramp in Fig. 11 are spread out over a single *St* range and clearly show the suppression of all peaks above 90 dB.

5. Bevels

These suppressor experiments have employed blocks that are bevelled along one edge across the full height of the block perpendicular to the airflow. The bevel drops *h* used are 0.25, 0.5, 1.0, and 1.5 cm, corresponding to $h/d = \frac{1}{8}, \frac{1}{4}, \frac{1}{2}$, and $\frac{3}{4}$, respectively. The blocks are placed in the experimental set-up so that the bevelled edge is at the main duct–sidebranch interface as shown in Fig. 2. A total of seven experiments are conducted using bevels of various *h*'s along with square blocks upstream and downstream of the sidebranch as detailed in Table 2.

The first four experiments in Table 2 employ a pair of equal size bevels upstream and downstream of the sidebranch as detailed in Table 2. For a selected length and flow rate, Fig. 12 shows a typical comparison of inlet *SPL* for each bevel size and the square interface blocks. All of

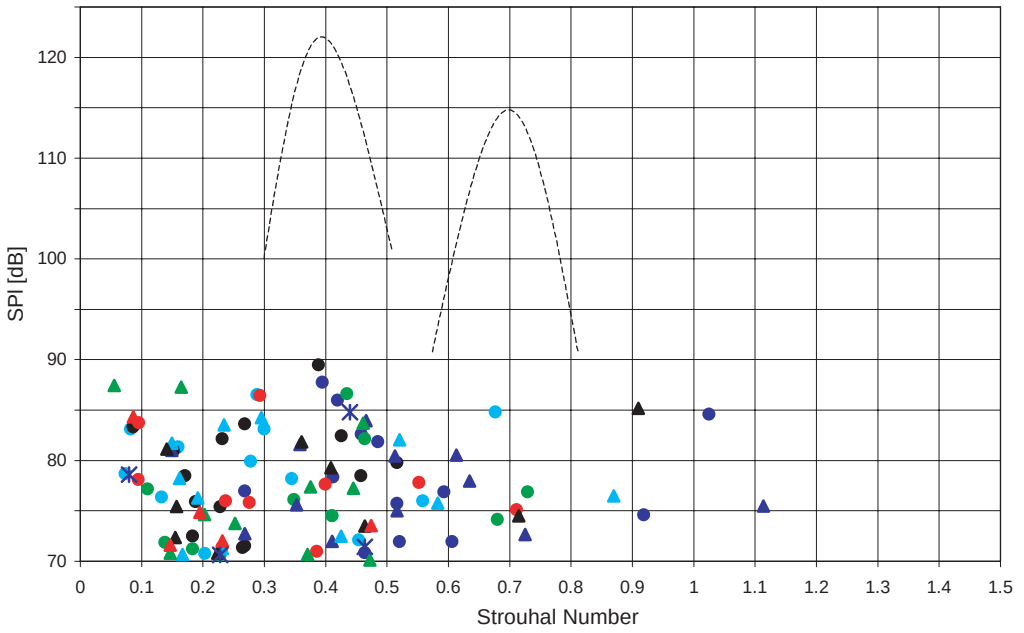

Fig. 11. Inlet *SPL* versus Strouhal number; variable sidebranch lengths, upstream $h/d = \frac{3}{4}$ ramp; length, L: ●, 0.05 m; ●, 0.1 m; ●, 0.2 m; ●, 0.3 m; ●, 0.4 m; ▲, 0.5 m; ▲, 0.6 m; ▲, 0.7 m; ▲, 0.8 m; ▲, 0.9 m; ✱, 1.0 m.

Table 2
Block configurations for bevel suppressor experiments

Upstream	Downstream
$h/d = \frac{1}{8}$ bevel	$h/d = \frac{1}{8}$ bevel
$h/d = \frac{1}{4}$ bevel	$h/d = \frac{1}{4}$ bevel
$h/d = \frac{1}{2}$ bevel	$h/d = \frac{1}{2}$ bevel
$h/d = \frac{3}{4}$ bevel	$h/d = \frac{3}{4}$ bevel
$h/d = \frac{1}{8}$ bevel	Square
Square	$h/d = \frac{1}{8}$ bevel
Square	$h/d = \frac{1}{4}$ bevel

the bevel sizes may be observed to suppress the two baseline peaks at 1200 and 2400 Hz, but the bevels create a new peak around 450 Hz that is not present with the square interface. The normalized frequency of this new peak is $f_n = 1.1$, in comparison to $f_n = 2.9$ for the peak at 1200 Hz. This reduction in f_n of about 2 represents a drop of one mode in the quarter-wave resonances. For the same L and flow rate, Fig. 13 shows a behavior similar to that of Fig. 12 at the piston surface. The trends in Fig. 12 are representative of the entire range of flow rates and sidebranch lengths examined, which suggests that while the bevels may suppress peaks due to the square blocks with higher f_q, they may also introduce new peaks corresponding to lower f_q with amplitudes approaching or exceeding those of the suppressed

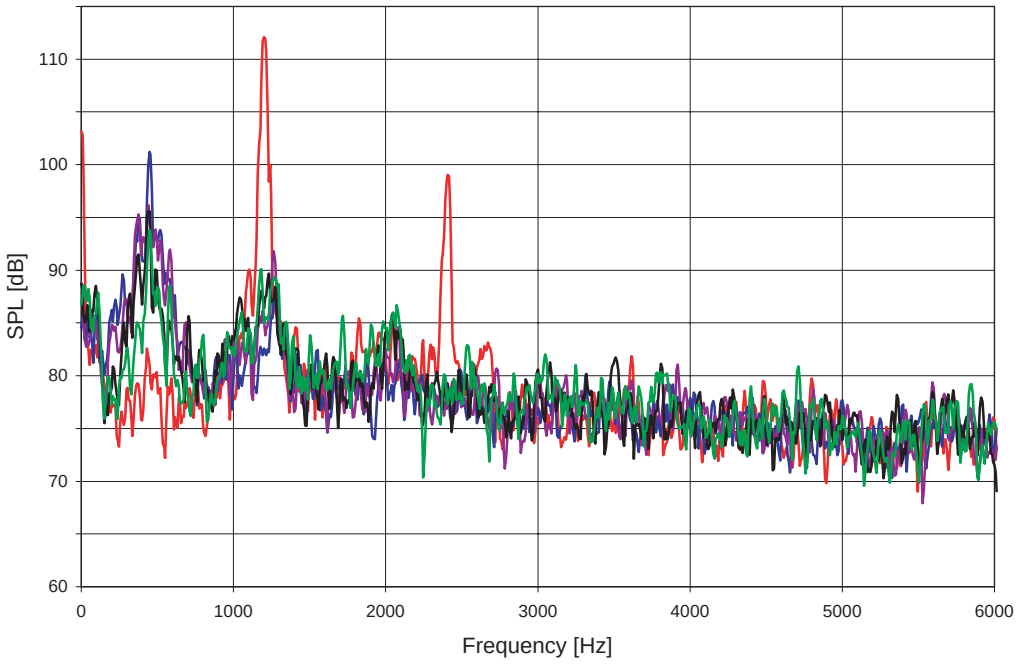

Fig. 12. Inlet *SPL* versus frequency; comparison of square with upstream and downstream bevelled interfaces, $L = 0.2$ m, 1000 cfm: ——, square; h/d: ——, $\frac{1}{8}$; ——, $\frac{1}{4}$; ——, $\frac{1}{2}$; ——, $\frac{3}{4}$.

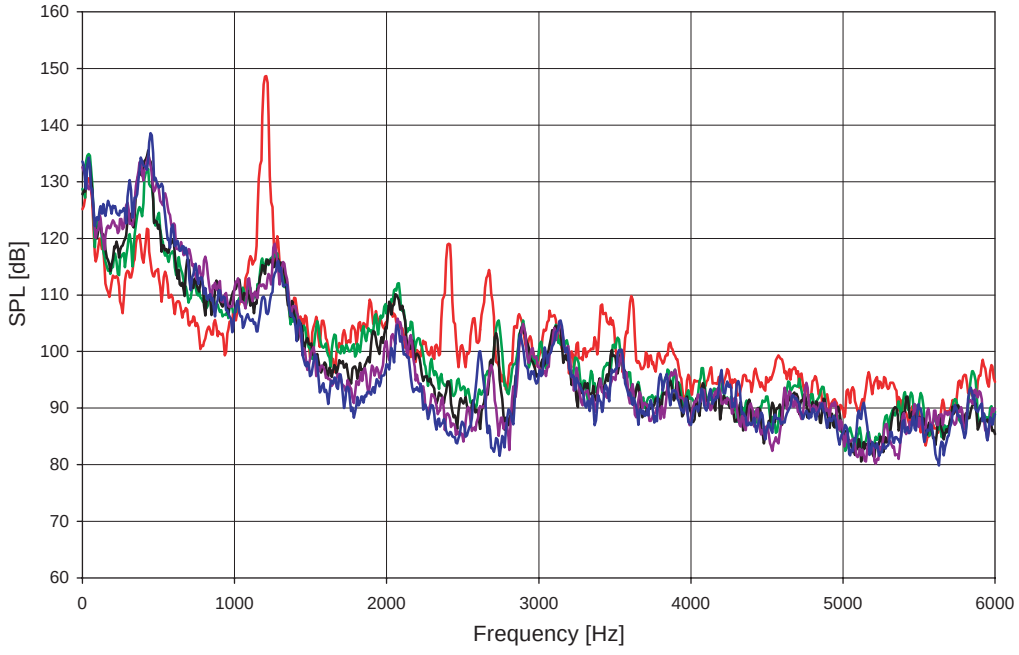

Fig. 13. Piston *SPL* versus frequency; comparison of square with upstream and downstream bevelled interfaces, $L = 0.2$ m, 1000 cfm: ——, square; h/d: ——, $\frac{1}{8}$; ——, $\frac{1}{4}$; ——, $\frac{1}{2}$; ——, $\frac{3}{4}$.

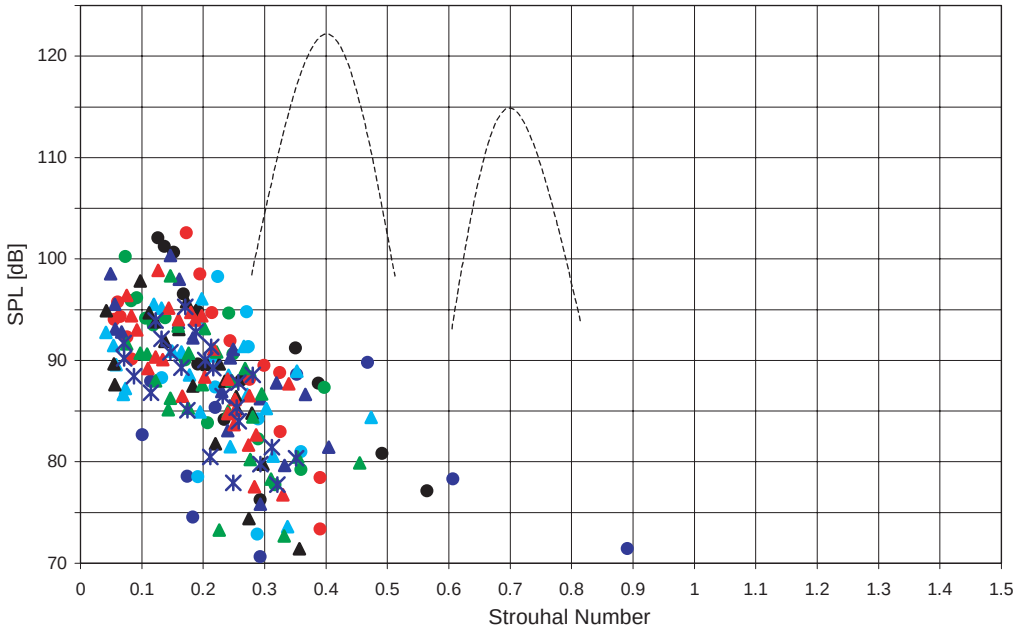

Fig. 14. Inlet *SPL* versus Strouhal number; variable sidebranch lengths, $h/d = \frac{3}{4}$ bevel edges; length, *L*: ●, 0.05 m; ●, 0.1 m; ●, 0.2 m; ●, 0.3 m; ●, 0.4 m; ▲, 0.5 m; ▲, 0.6 m; ▲, 0.7 m; ▲, 0.8 m; ▲, 0.9 m; ✱, 1.0 m.

peaks. All of the bevel sizes examined follow the same trends with the only difference among them being the larger bevels generally suppressing the baseline peaks by a few dB more than the smaller bevels and also creating new peaks that are a few dB higher than the smaller sizes.

Fig. 14 shows typical inlet *SPL* against Strouhal number results for all the bevel sizes examined, to be contrasted with the dashed lines (carried over from Fig. 4 for the square interface configuration). While the two distinct relatively narrow bands observed in Fig. 4 are centered near $St = 0.4$ and 0.70, the bevel results in Fig. 14 lie in a single band of about $St = 0.05$–0.3 for peaks above 90 dB.

The remaining three experiments in Table 2 with upstream-only and downstream-only bevels lead to different results, but each is similar to some earlier experiments. The upstream-only bevel shows similarity to the combined upstream and downstream bevel results in that: (1) the *SPL*s of the peaks are all reduced below 105 dB, suggesting that the upstream-only bevel is capable of suppressing high *SPL* peaks; and (2) there are a significant number of new peaks with *SPL*s above 90 dB and frequencies below 1500 Hz that are now generated by the upstream bevel itself. The downstream-only bevel results show that: (1) it is similar to the square interface results of Section 3 in terms of the general trends in dot graphs; (2) it does not cause any significant new peaks that represent a new source of noise; (3) unlike the upstream bevel, it does not suppress all of the high *SPL* peaks; and (4) the only effect of increasing the size of the downstream bevel is to slightly reduce the maximum amplitude.

6. Curved (radius) interface

Curved (radiused) edges have been among the subjects of previous works by Jungowski et al. [5] and Bruggeman et al. [2]. The effectiveness of this geometry on noise suppression is studied here in a 2-D duct set-up with varying radii. The experiments have been conducted using blocks that are rounded along one edge across the full height of the block perpendicular to the airflow. These blocks will hereafter be referred to as "radius" blocks. The radii used are $r = 0.5$, 1.0, 1.5, and 2.0 cm, corresponding to $r/d = \frac{1}{4}, \frac{1}{2}, \frac{3}{4}$, and 1, respectively. These blocks are placed in the experimental set-up so that the rounded edge is at the main duct–sidebranch interface as shown in Fig. 2. The same size radius block is mounted in both the upstream and downstream locations in each experiment.

Fig. 15 shows a typical comparison of the inlet *SPL* spectra from four radii and the square interface blocks for $L = 0.2$ m and 1000 cfm. These results are similar to those of the bevels in Fig. 12 in that the suppressor blocks reduce the highest baseline peaks below 95 dB, but also create new peaks at lower frequencies. The normalized frequency of the new radius peak $f_n = 1.1$ in Fig. 15 also corresponds to a quarter-wave frequency f_q similar to the new bevel peak in Fig. 12. While this similarity between the two types of suppressor blocks is not surprising in view of their somewhat comparable geometries, there are some differences between the two, including the *SPL* of the new peak at 450 Hz in Figs. 12 and 15 with $f_n = 1$ being 5 dB lower with the radius blocks, and the reduction in the amplitude of the new peaks for the smallest radius being a few dB lower.

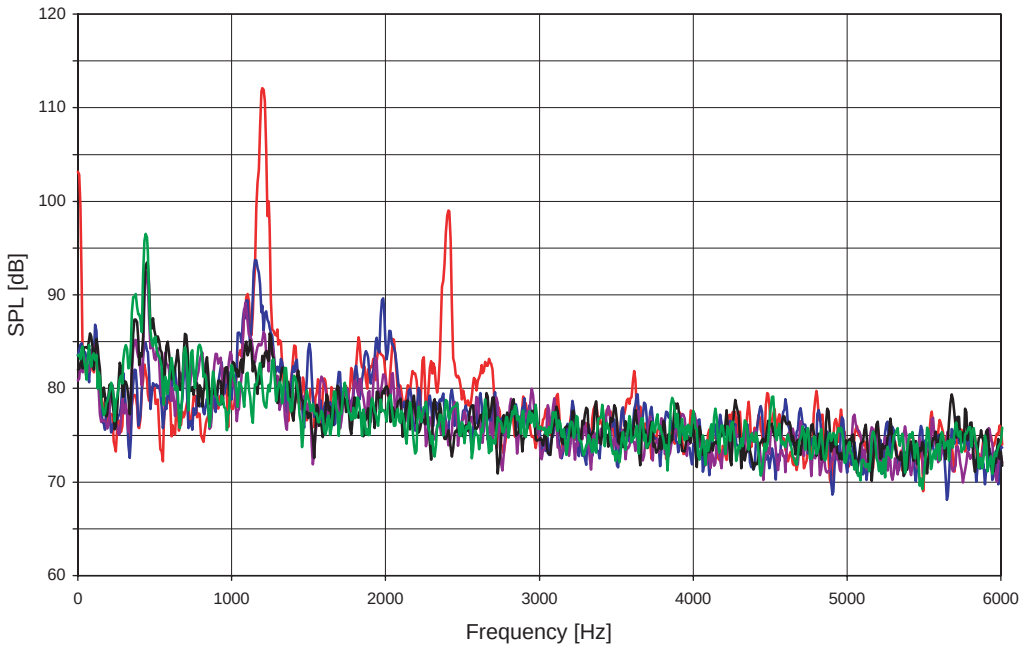

Fig. 15. Inlet *SPL* versus frequency; comparison of square with upstream and downstream radiused interfaces, $L = 0.2$ m, 1000 cfm: ——, square; r/d: ——, $\frac{1}{4}$; ——, $\frac{1}{2}$; ——, $\frac{3}{4}$; ——, 1.

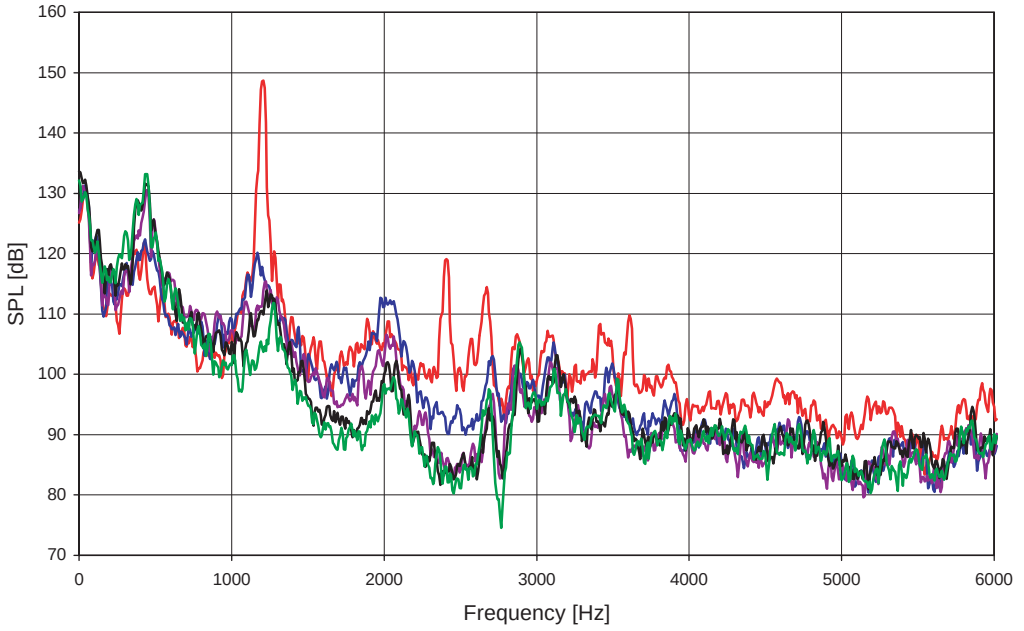

Fig. 16. Piston *SPL* versus frequency; comparison of square with upstream and downstream radiused interfaces, $L = 0.2$ m, 1000 cfm: ——, square; r/d: ——, $\frac{1}{4}$; ——, $\frac{1}{2}$; ——, $\frac{3}{4}$; ——, 1.

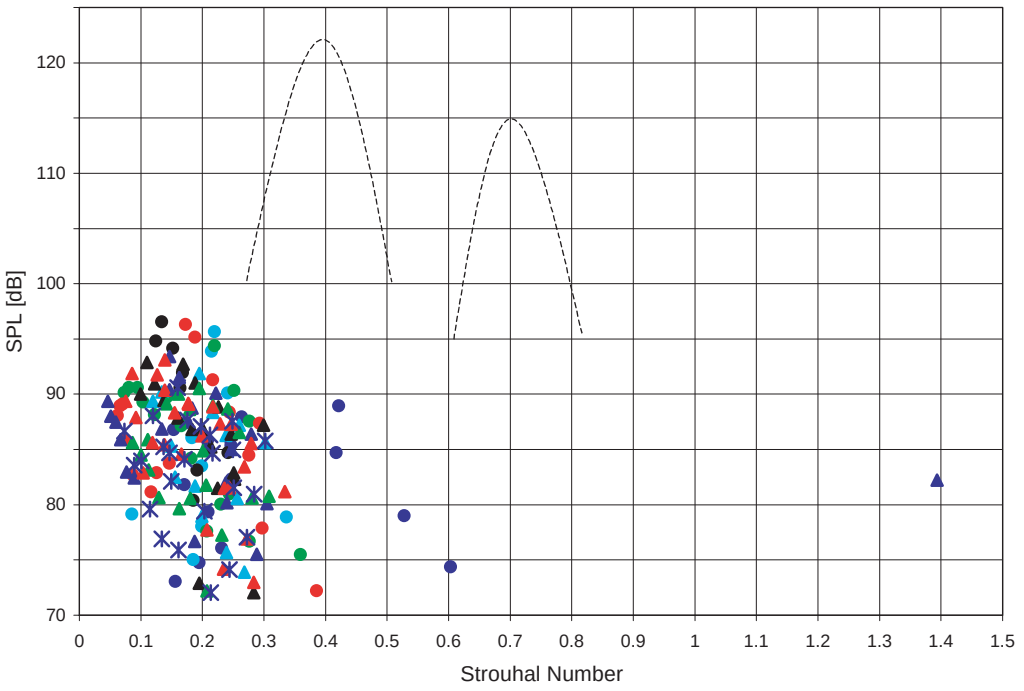

Fig. 17. Inlet *SPL* versus Strouhal number; variable sidebranch lengths, $r/d = 1$ radius; length, L: ●, 0.05 m; ●, 0.1 m; ●, 0.2 m; ●, 0.3 m; ●, 0.4 m; ▲, 0.5 m; ▲, 0.6 m; ▲, 0.7 m; ▲, 0.8 m; ▲, 0.9 m; ✱, 1.0 m.

These differences are applicable over the entire range of flow rates examined. Fig. 15 suggests that, similar to the bevel blocks, the radius blocks will suppress most high *SPL* baseline peaks, but will create new peaks at f_n's lower than those of the baseline peaks. The new peaks have f_n's corresponding to the first couple f_q's with amplitudes lower than the unsuppressed baseline peaks. For the same L and flow rate, Fig. 16 illustrates that the trends in Fig. 15 are, in general, also observed at the piston surface.

Fig. 17 shows typical *SPL* against Strouhal number data for the largest ($r/d = 1$) radius experiments, to be contrasted with Fig. 4 for the square interface configuration. This figure shows the reduction in the number of peaks higher than 100 dB. The radius blocks, in general, tend to eliminate the second (higher *St*) band of the square blocks in Fig. 4. The central *St* of the primary band decreases with increasing radius. This decrease in peak *St* with increasing radius is comparable to the results of similar radius experiments by Jungowski et al. [8], and is also similar to the effect of increasing bevel size.

7. Concluding remarks

The effect of modifying the main duct–sidebranch interface of a quarter-wave resonator on the suppression of noise due to flow–acoustic coupling has been examined in this study. A two-dimensional, rectangular set-up consisting of a main duct with a connected closed sidebranch is fabricated to conduct the experiments on a flow stand. The main duct–sidebranch interface is modified using interchangeable blocks of varying shapes and sizes, including blocks with sharp edges, ramps, bevelled edges, and curved (radiused) edges. The external and internal sound pressure level measurements are analyzed to determine the effectiveness of the suppressors in reducing the flow–acoustic noise.

To provide a baseline for comparison with the suppressors, the sharp-edge square blocks are examined first with the following observations: (1) the *SPL* against *St* data show two constant *St* bands, one at about $St = 0.4$ and the other with slightly lower maximum *SPL* near $St = 0.7$, which generate the two bands in the variation of peak frequency against *Ma*; (2) the frequencies of these constant-slope bands increase with increasing *Ma* to maintain the constant *St* at which flow–acoustic coupling occurs; and (3) the *SPL* against normalized frequency f_n data show that a substantial number of peaks falls within a few Hz of the quarter-wave frequencies f_q of the sidebranch, suggesting the flow–acoustic coupling as the primary source of these peaks.

The first type of suppressor employs ramps of varying sizes ($h/d = \frac{1}{8}, \frac{1}{4}, \frac{1}{2}$, and $\frac{3}{4}$) spanning the full height of the main duct. These ramp blocks are placed upstream of the main duct–sidebranch interface to direct the airflow away from the sidebranch opening in an attempt to suppress the pure tones. All of the ramps examined suppress the high-amplitude baseline peaks. The larger two ramps ($h/d = \frac{1}{2}$ and $\frac{3}{4}$) suppress all peaks above 90 dB with no other significant effect, whereas the smaller two ramps ($h/d = \frac{1}{8}$ and $\frac{1}{4}$) create new peaks at frequencies corresponding to an increase of one quarter-wave mode over the strongest baseline peak. High amplitudes generated by the small ramps are likely to make them just as undesirable as the square blocks.

The second suppressor uses bevelled edges of varying sizes ($h/d = \frac{1}{8}, \frac{1}{4}, \frac{1}{2}$, and $\frac{3}{4}$). The experimental results from the bevel pairs upstream and downstream of the sidebranch opening suggest that: (1) all the bevel sizes investigated are effective at suppressing the significant peaks

due to the square blocks by at least 10–15 dB; and (2) the bevels create new peaks at frequencies that are generally lower than those of the baseline peaks and correspond to $f_q < 1$ kHz. Experiments conducted with the $h/d = \frac{1}{8}$ bevel in either the upstream or downstream position paired with a square interface block suggest that: (1) the suppression of high *SPL* baseline peaks and creation of new peaks by the upstream bevel is similar to the bevel pairs; (2) the downstream bevel does not generate any significant new peaks and does not suppress all of the high-amplitude baseline peaks; and (3) the only effect of increasing the size of the downstream bevel is to slightly reduce the maximum amplitude.

The third suppressor uses radiused edges of varying sizes ($r/d = \frac{1}{4}, \frac{1}{2}, \frac{3}{4}$, and 1) mounted in pairs upstream and downstream of the sidebranch interface. These radiused blocks produce results similar to those of the bevels, such as: (1) suppressing all of the strong baseline peaks; and (2) introducing new peaks at frequencies corresponding to lower f_q than the strongest baseline peaks for the same configuration. The new peaks introduced by the radii generally have the same frequencies as those of the bevels, however the radius peaks tend to be about 5 dB lower in maximum *SPL* than those generated by the bevels. These results suggest that while the radius sizes examined are generally effective at suppressing the baseline peaks at high amplitudes they also create new ones at lower frequencies.

The suppression methods investigated in this study have varying levels of effectiveness. The two largest ramps examined have been determined as the most effective for suppressing the peaks generated by flow–acoustic coupling, while not introducing significant new peaks at different frequencies. The radiused, or curved, blocks are the next most effective suppressors, with the larger radii somewhat better than the smaller sizes, while the bevels are slightly less effective than the radiused blocks. The suppression methods examined may produce different results with variations in the size and configuration of the sidebranch. Future work on suppressors could focus on a number of areas, including different combinations and sizes of bevels, ramps, and radii, different configurations of sidebranches, flow perturbations in the main duct upstream of the interface, and different flow conditions such as increased flow rates. For an effective suppressor, it must be ensured that the method employed does not create significant new tones, while weakening or eliminating the undesirable peaks due to flow–acoustic coupling.

Appendix A. Nomenclature

a	ramp or bevel length
c	speed of sound
d	sidebranch width; sidebranch diameter [8]
D_H	hydraulic diameter
D_{main}	main duct diameter
f	frequency
h	ramp or bevel height
L	sidebranch length
Ma	Mach number
p	pressure
r	rounding radius

R	specific gas constant
Re	Reynolds number
St	Strouhal number
T	temperature
U	average velocity in the main duct
γ	ratio of specific heats
v	kinematic viscosity

Subscripts

c	corrected
n	normalized
q	quarter-wave
$r.m.s.$	root mean square

References

[1] D. Rockwell, E. Naudascher, Review—self sustaining oscillations of flow past cavities, Transactions of the American Society of Mechanical Engineers, Journal of Fluids Engineering 100 (1978) 152–165.
[2] N.M. Komerath, K.K. Ahuja, F.W. Chambers, Prediction and measurement of flows over cavities—a survey, American Institute of Aeronautics and Astronautics Paper No. 87-0166, American Institute of Aeronautics and Astronautics 25th Aerospace Sciences Meeting, Reno, NV, January 12–25, 1987.
[3] M.E. Franke, D.L. Carr, Effect of geometry on open cavity flow-induced pressure oscillations, American Institute of Aeronautics and Astronautics Paper No. 75-492, 1975.
[4] H.H. Heller, D.B. Bliss, Flow-induced pressure fluctuations in cavities and concepts for their suppression, American Institute of Aeronautics and Astronautics Paper No. 75-491, 1975.
[5] L.L. Shaw, Suppression of aerodynamically induced cavity pressure oscillations, Journal of the Acoustical Society of America 66 (1979) 880–884.
[6] R.L. Sarno, M.E. Franke, Suppression of flow-induced pressure oscillations in cavities, American Institute of Aeronautics and Astronautics Paper No. 90-4018-CP, 1990.
[7] R.M. Baldwin, H.R. Simmons, Flow-induced vibration in safety relief valves, Journal of Pressure Vessel Technology 108 (1986) 267–272.
[8] W.M. Jungowski, K.K. Botros, W. Studzinski, Cylindrical side-branch as tone generator, Journal of Sound and Vibration 131 (1989) 265–285.
[9] J.C. Bruggeman, A. Hirschberg, M.E.H. Van Dongen, A.P.J. Wijnands, J. Gorter, Self-sustained aero-acoustic pulsations in gas transport systems: experimental study of the influence of closed side branches, Journal of Sound and Vibration 150 (1991) 371–393.
[10] S.F. Mcgrath, D.J. Olinger, Control of pressure oscillations in deep cavities excited by grazing flow, Journal of Aircraft 33 (1996) 29–36.
[11] B.D. Knotts, Suppression of Flow–Acoustic Coupling in Sidebranch Ducts by Interface Modification, M.S. Thesis, The Ohio State University, 2000.
[12] P.M. Radavich, A. Selamet, J.M. Novak, A computational approach for flow–acoustic coupling in closed side branches, Journal of the Acoustical Society of America 109 (2001) 1343–1353.
[13] J.W.S. Rayleigh, The Theory of Sound, Vol. II, Art. 293, Dover, New York, 1945.